Published in Chemistry – A European Journal, Vol. 22, Issue 48, 2016, p. 17366-17376
which should be used for any reference to this work

Design, Synthesis, and Self-Assembly Behavior of Liquid-Crystalline Bis-[60]Fullerodendrimers

Virginie Russo,[a] Pauline Pieper,[a] Benoît Heinrich,[b] Bertrand Donnio,*[b] and Robert Deschenaux*[a]

Abstract: Bis-[60]fullerodendrimers were synthesized by assembling [60]fullerene-containing type I (terminal olefin) and type II (α,β-unsaturated carbonyl olefin) olefins through the olefin cross-metathesis reaction. The synthetic modular approach developed in this study allowed the preparation of mono-[60]fullerodendrimers and their [60]fullerene-free analogues. First- and second-generation poly(aryl ester) dendrons carrying cyanobiphenyl mesogens were used as liquid-crystalline promoters. The liquid-crystalline properties were studied by polarized optical microscopy, differential scanning calorimetry, and small-angle X-ray scattering. In agreement with the nature and structure of the dendrimers, nematic, smectic, and multisegregated lamellar phases were observed. Owing to its versatility and tolerance towards many functional groups, olefin cross-metathesis proved to be a reaction of choice for the elaboration of molecular materials with complex architectures.

Introduction

The design of functional materials for the elaboration of high-performance supramolecular devices that display specific properties is both a conceptual and synthetic challenge.[1] Within this context, [60]fullerene (C_{60}), an exceptional photophysical[2] and electrochemical[3] unit, generated exciting studies in medicinal[4] (DNA photocleavage,[5] enzyme inhibition,[6] virus inhibition,[7] neuroprotection,[8] antibacterial activity[9]) and materials science (photoactive dyads,[10] triads,[11] polyads,[12] and plastic solar cells[13]). To improve the effectiveness of [60]fullerene-based devices, materials containing two,[14] three,[15] four,[16] or more[17] C_{60} units were synthesized. Such compounds are also interesting from the point of view of synthetic chemistry. Indeed, their synthesis requires the precise control of the reactivity and stereochemistry of [60]fullerene. For example, oligophenylene ethynylene (OPE)/oligophenylene vinylene (OPV) oligomers were functionalized with bis-(fullerenyl) end-capping groups.[18] The length of the oligomeric OPE/OPV bridge between the two C_{60} units was varied. Substantially quenched fluorescence of the bridge was observed, which indicated rapid photoinduced intramolecular energy/electron transfer. Fulleropyrrolidine end-capped molecular wires are other interesting bis-[60]fullerene derivatives.[19] A short bridge was used to connect two C_{60} units. The compound with a benzene bridge behaved as a molecular wire. A light-absorbing π-conjugated oligomer–tetrafullerene nanoarray was synthesized and its photophysical properties investigated.[16a] Intramolecular energy transfer was observed. A photovoltaic device fabricated from this compound and poly(3-hexylthiophene) showed a high external quantum efficiency at $\lambda = 500$ nm. Finally, dendrimers containing 1, 2, 4, 8, or 16 C_{60} units were reported.[17a] The [60]fullerene-based dendrimers formed clusters when solutions of the dendrimers in toluene were injected into acetonitrile. The clusters were deposited onto SnO_2-coated indium tin oxide (ITO) electrodes. The photovoltaic efficiency increased with the number of C_{60} units. On the other hand, the functionalization of C_{60} with liquid-crystalline or non-liquid-crystalline addends through addition reactions (e.g., the Bingel reaction[20] or the 1,3-dipolar cycloaddition reaction[21]) opened up avenues for the design of innovative self-assembling materials.[22] Based on the above-mentioned reactions, liquid-crystalline fullerenes have been reported, such as alkylated [60]fullerenes,[23] liquid-crystalline hexa-adducts of [60]fullerene,[24] liquid-crystalline derivative of $Y_3N@C_{80}$,[25] amphiphilic oligothiophene–[60]fullerene dyads,[26] [60]fullerene-based bent-core liquid crystals,[27] and liquid-crystalline [60]fullerene–oligophenylenevinylene conjugates.[28] The above-mentioned fullerene derivatives gave rise to nematic, smectic, columnar, and cubic phases. With the exception of a bis-[60]fullerene–porphyrin material, for which a triclinic unit cell was obtained,[29] all [60]fullerene-containing liquid crystals reported so far contain only one C_{60} unit. This is because the incorporation of two (or more) C_{60} units within mesomorphic architectures is a difficult synthetic task that requires perfect control of the molecular design for

[a] *V. Russo, P. Pieper, Prof. R. Deschenaux*
Institut de Chimie, Université de Neuchâtel
Avenue de Bellevaux 51, 2000 Neuchâtel (Switzerland)
E-mail: robert.deschenaux@unine.ch

[b] *Dr. B. Heinrich, Dr. B. Donnio*
Institut de Physique et Chimie des Matériaux de Strasbourg (IPCMS)
UMR 7504, CNRS-Université de Strasbourg
23 rue du Lœss, BP 43, 67034 Strasbourg Cedex 2 (France)
E-mail: bdonnio@ipcms.unistra.fr

Supporting information and ORCID from the author for this article are available on the WWW under http://dx.doi.org/10.1002/chem.201603408.

mesomorphism to develop.[28] This challenge motivated us to develop synthetic pathways that would lead to liquid-crystalline bis-[60]fullerene derivatives.

Recently, we applied the olefin cross-metathesis reaction[30] to synthesize Janus liquid crystals[31] and liquid-crystalline gold nanoparticles (AuNPs).[32] In the former study, mesomorphic or non-mesomorphic type I (terminal olefin) and type II (α,β-unsaturated carbonyl olefin) olefins were linked together; in the latter study, mesomorphic type II olefins were grafted onto AuNPs functionalized with type I olefins. In both cases, the olefin cross-metathesis reaction was carried out under standard conditions with control of the stereochemistry of the carbon–carbon double-bond formed in the cross-metathesis products (*E* configuration). The observed liquid-crystalline properties were in agreement with the structure and nature of the olefinic precursors (smectic A, nematic, and chiral nematic phases). Based on those studies, we anticipated that olefin cross-metathesis would be an ideal reaction to link two liquid-crystalline building blocks, each of which containing a C_{60} unit.

We report herein the synthesis, characterization, mesomorphic properties, and supramolecular organization of first- (**1**; Figure 1) and second-generation (**5**; Figure 2) bis-[60]fullerodendrimers, and their [60]fullerene-free and mono-[60]fullerene analogues, obtained by olefin cross-metathesis reactions between type I (terminal olefins) and type II (α,β-unsaturated carbonyl olefins) olefinic molecular modules. A comparison of their liquid-crystalline properties allowed us to understand the role played by the C_{60} units on the formation, structure, and stability of the mesophases.

Results and Discussion

The design of the title compounds is based on the functionalization of C_{60} with first- and second-generation poly(arylester) dendrons carrying cyanobiphenyl (CB) groups as liquid-crystalline promoters. Such dendromesogens were selected to generate layered mesophases. [60]Fullerene is added to olefinic malonate derivatives through the Bingel reaction.[20] Finally, the olefinic frameworks were assembled by applying the olefin cross-metathesis reaction in the presence of second-generation Grubbs catalysts.[30]

The preparation of bis-[60]fullerodendrimers **1** (Figure 1) and **5** (Figure 2) first required the synthesis of olefinic precursors. The preparation of first-generation olefins is shown in Scheme 1. The reaction of alcohol **7**[33] with Meldrum acid (2,2-dimethyl-1,3-dioxane-4,6-dione) gave carboxylic acid **8**. Esterifi-

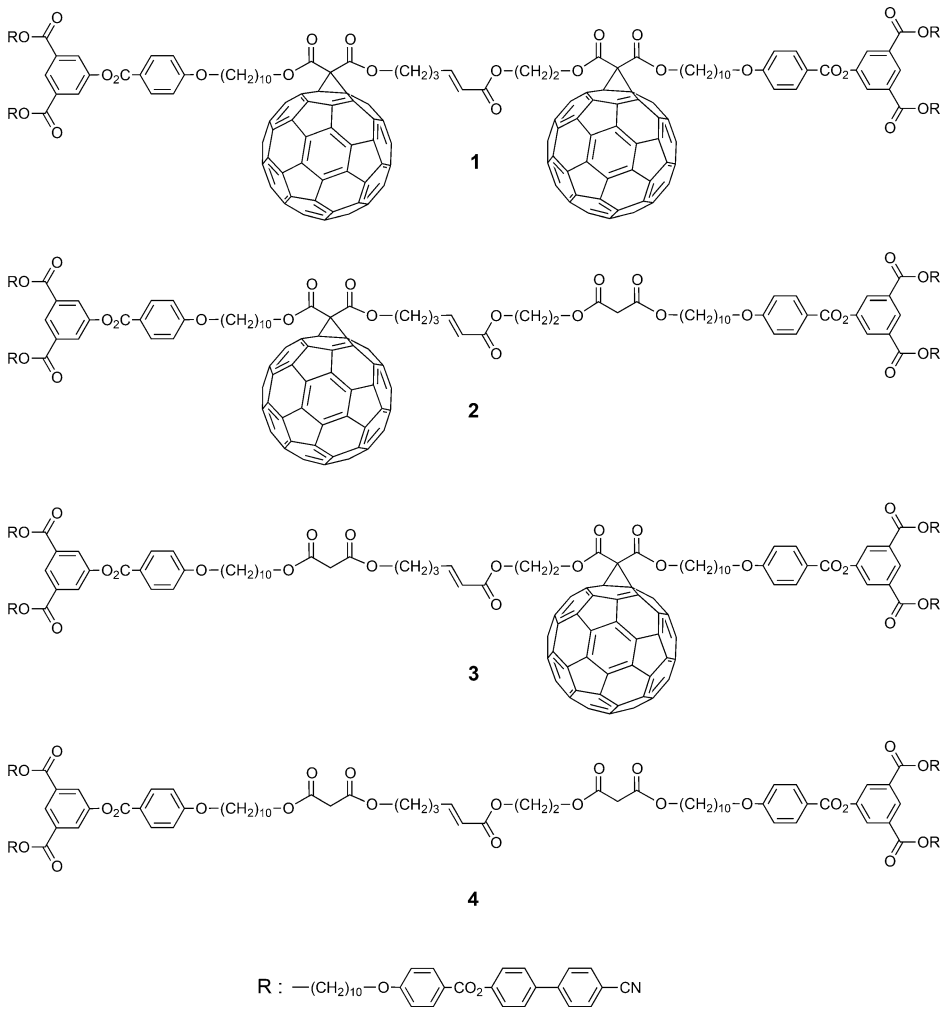

Figure 1. Structures of first-generation bis-[60]fullerodendrimer **1** and related materials.

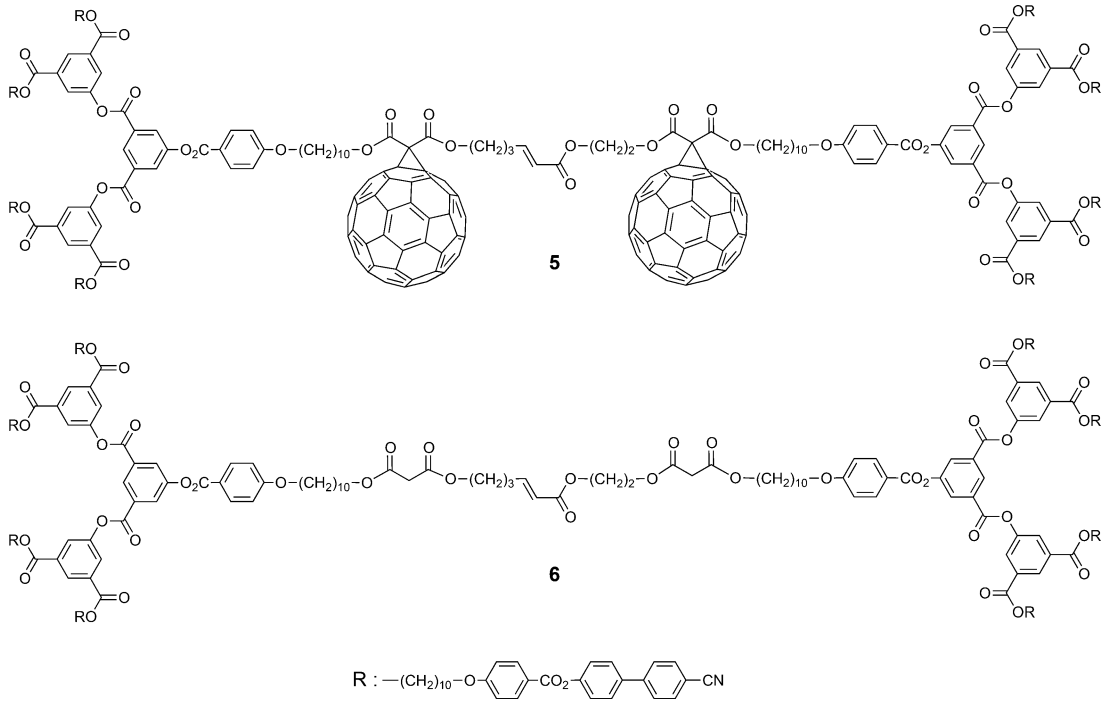

Figure 2. Structures of second-generation bis-[60]fullerodendrimer **5** and bis-malonate **6**.

cation of the latter with either 4-penten-1-ol or 2-hydroxyethyl acrylate in the presence of DCC and DPTS in dry CH_2Cl_2 gave malonates **9** and **10**, respectively. Cyclopropanation of C_{60} with malonate **9** or **10** under modified Bingel conditions[20] gave mono-[60]fullerene derivatives **11** and **12**, respectively. Second-generation olefinic malonates **15** and **16**, and mono-[60]fullerenes **17** and **18** were synthesized by analogy to the first-generation dendrons, as shown in Scheme 2.

Target materials **1**–**6** were synthesized by an olefin cross-metathesis reaction between olefins of type I (**9**, **11**, **15**, and **17**) and type II (**10**, **12**, **16**, and **18**). In a typical procedure (Scheme 3), a mixture of type I (1 equiv) and type II (1.1–1.5 equiv) olefins in dry CH_2Cl_2 was stirred at 40 °C for 16 h in the presence of second-generation Grubbs catalyst (0.1 equiv) and CuI[34] (0.06 equiv). Compounds containing one or two C_{60} units, **1**–**3** and **5**, were purified by gel permeation chromatography (Biobeads SX-1, toluene) and column chromatography (silica gel, CH_2Cl_2/EtOAc, 100:0 to 100:5). Bis-malonates **4** and **6** were purified by column chromatography (silica gel, CH_2Cl_2/EtOAc, 100:0 to 100:6). All compounds were precipitated in MeOH. The yields of the olefin cross-metathesis compounds after purification ranged from 44 to 53% for the first-generation dendrimers, and from 26 to 38% for the second-generation dendrimers.

The *E* configuration of the newly formed carbon–carbon double bond in compounds **1**–**6** was established by ^{1}H NMR spectroscopy. An example is illustrated in Figure 3. The ^{1}H NMR spectrum of bis-malonate **4** showed two doublets of triplets at $\delta = 6.96$ and 5.86 ppm, corresponding to the olefinic protons H_b and H_a, respectively. From the signal at $\delta = 5.86$ ppm, the $^3J_{trans}$ coupling constant between the two olefinic protons H_a and H_b was obtained. The value of 15.7 Hz confirmed the *E* configuration of the carbon–carbon double bond.

Type II olefin was added in excess because the cross-metathesis reaction was in competition with the dimerization of type I olefins. Despite this precaution, homodimerization products were obtained in some reactions. For example, during the synthesis of compound **1**, the homodimer of **11** was identified by mass spectrometry and ^{1}H NMR spectroscopy (with a signal at $\delta = 5.55$ ppm). In all cases, the homodimers were eliminated during purification.

The structures and purities of all compounds were confirmed by NMR spectroscopy, mass spectrometry, and elemental analysis. The UV/Vis spectra of **1** and **3** are shown as representative examples in Figure 4. Three absorption bands, which are characteristic for mono-adducts of C_{60},[35] were observed at $\lambda \approx 425$, 485, and 685 nm for both compounds. Finally, the C_{60} derivatives retained the solubility properties of the corresponding malonates and were soluble in common organic solvents.

Liquid-crystalline behavior

The liquid-crystalline and thermal properties of the cross-metathesis compounds **1**–**6** and olefin precursors **9**, **11**, **15**, and **17** were investigated by polarized optical microscopy (POM), differential scanning calorimetry (DSC), and small-angle X-ray scattering (SAXS). The phase-transition temperatures and enthalpy changes are reported in Table 1. The thermal behavior of type II olefins (compounds **10**, **12**, **16**, and **18**) was not investigated because such acrylate derivatives readily polymerize when heated.[31]

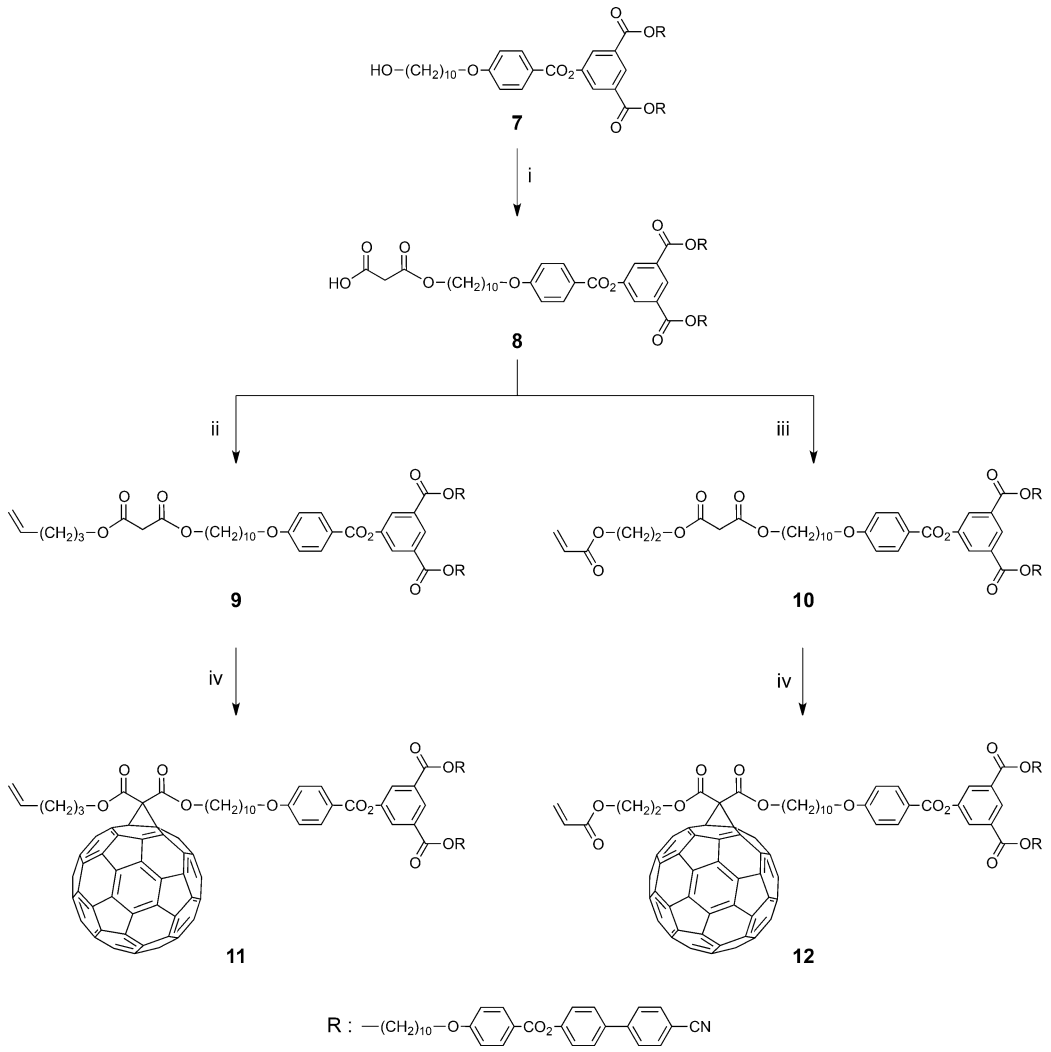

Scheme 1. Reagents and conditions: i) Meldrum acid, toluene, 65 °C, 24 h, 98%; ii) 4-penten-1-ol, *N*,*N*′-dicyclohexylcarbodiimide (DCC), 4-dimethylaminopyridinium *p*-toluenesulfonate (DPTS), dry CH_2Cl_2, RT 20 h, 86%; iii) 2-hydroxyethyl acrylate, DCC, DPTS, dry CH_2Cl_2, RT 20 h, 71%; iv) C_{60}, I_2, 1,8-diazabicyclo[5.4.0] undec-7-ene (DBU), toluene, RT 4 h, 59 (**11**) and 62% (**12**).

As revealed by POM, all of the compounds displayed mesomorphic behavior. Textures typical of tilted (schlieren texture) and orthogonal (focal-conic fan texture and homeotropic areas) smectic phases were observed. Type I olefins **9** and **15** and bis-malonate derivatives **4** and **6** also gave rise to nematic (N) phases. It is noteworthy that bis-[60]fullerodendrimers **1** and **5** showed only the formation of one mesophase. Illustrative examples of optical textures are presented in Figures 5–8. The emergence of lamellar phases is in agreement with the structure and nature of the molecules that carry CB mesogens. Indeed, such calamitic mesogens tend to align parallel one to each other to form layers and lead to the formation of layered organizations. Moreover, the multiblock molecular architecture encountered for C_{60} derivatives (compounds **11**, **17**, **1**–**3**, and **5**) implies segregation of the various molecular constituents (i.e., CB units, appended [60]fullerenes, dendritic arborescence, and aliphatic spacers) into multisegregated lamellar architectures.[33, 36, 37]

A comparison of the liquid-crystalline properties of mono-[60]fullerodendrimers, bis-[60]fullerodendrimers, and malonate derivatives gives clues to understand the effect of C_{60} on the stability of the mesophases.

On one hand, the clearing points of mono-[60]fullerodendrimers **2** (156 °C) and **3** (156 °C) are lower than that of their malonate precursor **4** (175 °C). This behavior is in agreement with results obtained for other mono-[60]fullerene derivatives[37] and is an indication that insertion of one C_{60} unit per mesomorphic molecule tends to lower the stability of the mesophases, most likely, because of strong perturbations in the layered structure. On the other hand, the clearing point of bis-[60]fullerodendrimers **1** (168 °C) and **5** (175 °C) are close to those of the corresponding malonates **4** (175 °C) and **6** (180 °C), respectively. This behavior can be attributed, at least in part, to C_{60}–C_{60} interactions, and reveals a beneficial effect of the C_{60} content (more than one C_{60} unit per mesomorphic molecule) on the stability of the mesophases.

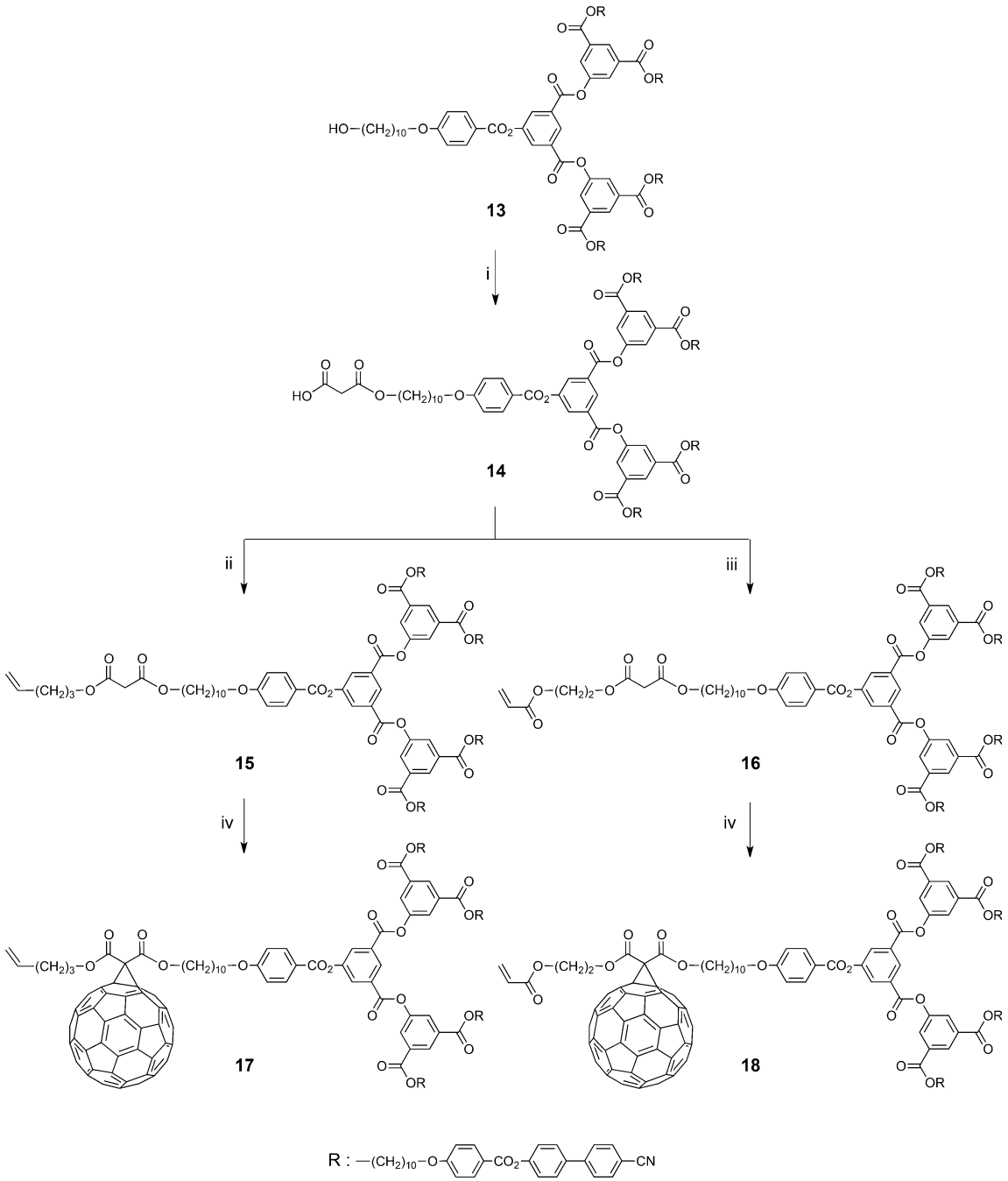

Scheme 2. Reagents and conditions: i) Meldrum acid, toluene, 65 °C, 24 h, 98%; ii) 4-penten-1-ol, DCC, DPTS, dry CH_2Cl_2, RT 20 h, 77%; iii) 2-hydroxyethyl acrylate, DCC, DPTS, dry CH_2Cl_2, RT 20 h, 66%; iv) C_{60}, I_2, DBU, toluene, RT 4 h, 24 (**17**) and 31% (**18**).

SAXS investigations

SAXS experiments were carried out at various temperatures (Figure 9, Table 2, and Figures S31–37 in the Supporting Information). In the pristine state, the self-organization structures were not well developed and the corresponding SAXS patterns consisted solely of small- and large-angle diffuse scatterings. However, upon heating the samples, the SAXS patterns evolved and now contained one or two sharp reflections in the small-angle region, and even up to three peaks for isomeric mono-[60]fullerodendrimers **2** and **3**, in the 1:2(:3) ratio; this unambiguously confirmed the formation of lamellar structures (Figure 9).

In addition, the patterns displayed several diffuse halos that occurred from liquid-like lateral interactions within the various sublayers. The strong halo in the wide-angle region, with a maximum at 4.4–4.6 Å, was readily assigned to the overlapping scattering signals from distances between molten aliphatic chains (h_{ch}) and mesogens (h_{mes}). For the C_{60} derivatives, an additional weak scattering was visible at about 10 Å (h_{ful}), which was thought to arise from loosely intercalated neighboring [60]fullerenes within the sublayers. Another broad signal

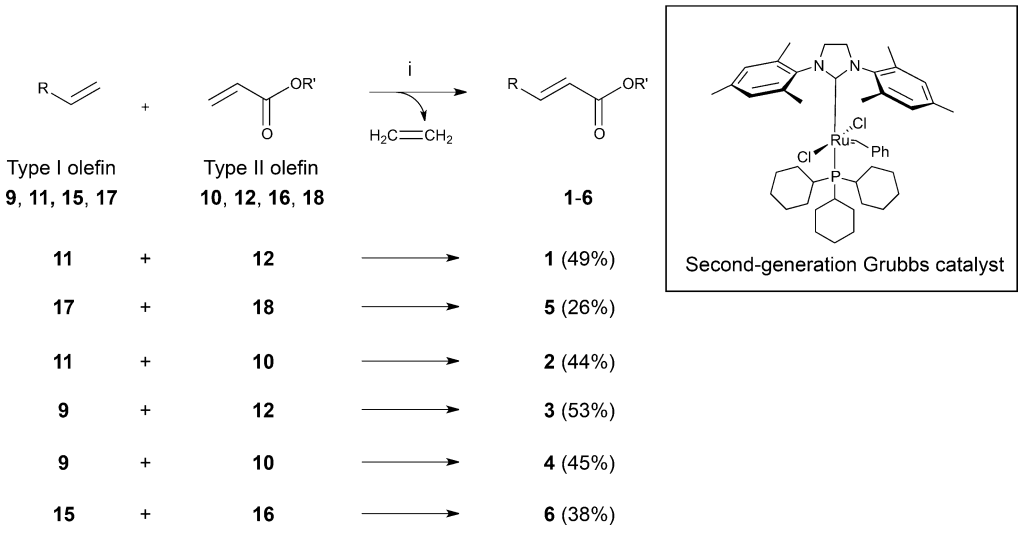

Scheme 3. Olefin cross-metathesis reaction and the structure of the second-generation Grubbs catalyst. Reagents and conditions: i) second-generation Grubbs catalyst (0.1 equiv), CuI (0.06 equiv), dry CH_2Cl_2, 40 °C, 16 h.

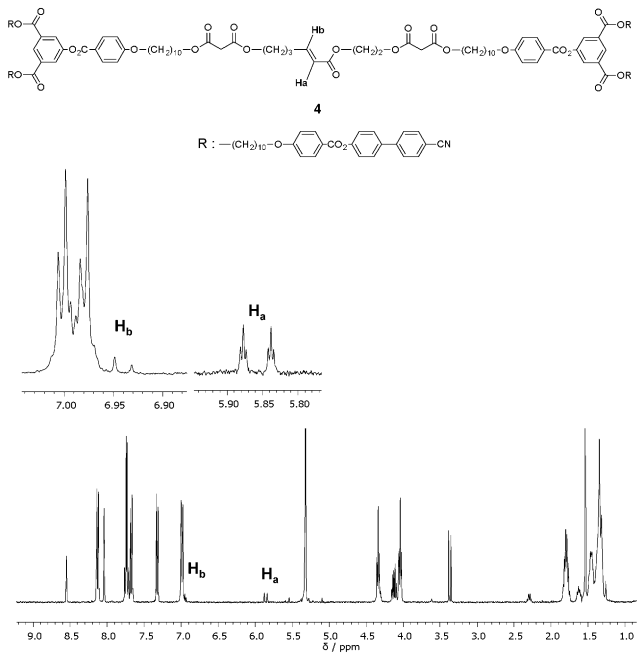

Figure 3. ^{1}H NMR spectrum (400 MHz, CD_2Cl_2) of bis-malonate **4**.

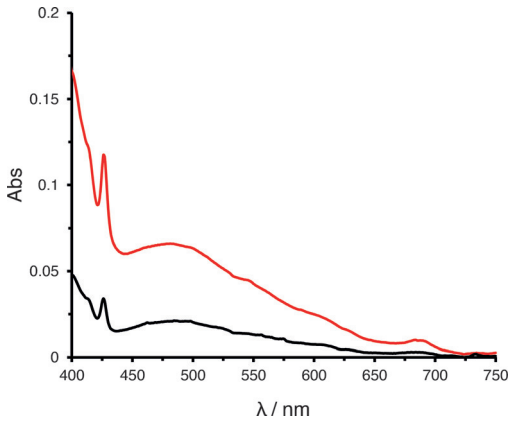

Figure 4. UV/Vis spectra of bis-[60]fullerodendrimer **1** (red) and mono-[60]fullerodendrimer **3** (black) in CH_2Cl_2.

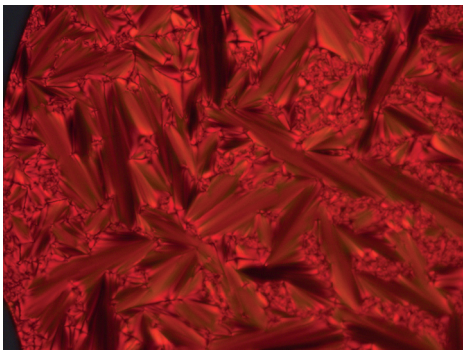

Figure 5. Thermal polarized optical micrograph of the focal-conic fan texture displayed by **11** in the mesophase at 147 °C.

(D) in the small-angle region, superimposed on or close to the sharp higher-order reflections of the lamellae, was observed for the second-generation compounds, and was assigned to loose distances between the protean dendritic skeletons. Finally, inversion of the distribution of the peak intensities was observed between the malonate and C_{60} derivatives and was in agreement with the intercalation of an electron-rich median strata within the mesophases (arising from C_{60} moieties hanging in the middle of the molecule). Thus, on the basis of SAXS and POM experiments, it can be concluded that dendritic addends **4** and **6** (and their precursors **9** and **15**) form "classical" SmA/C phases, consisting of the regular alternation of mesogenic and liquid-like sublayers (i.e., made of undifferentiated molten alkyl spacers and arylester parts). As for the corresponding C_{60} adducts, they generate multisegregated lamellar phases with the intercalation of a median [60]fullerene-rich

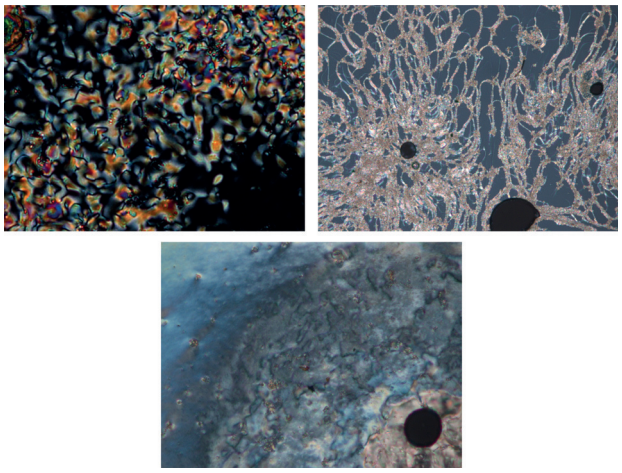

Figure 6. Thermal polarized optical micrographs of the schlieren texture (top left), the focal-conic and myelinic textures and homeotropic areas (top right), and the schlieren texture (bottom) displayed by **4** in the mesophases at 173, 150, and 79 °C, respectively.

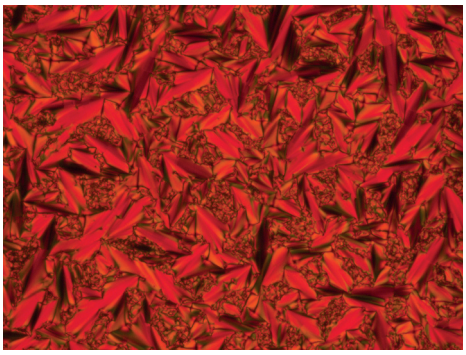

Figure 7. Thermal polarized optical micrograph of the focal-conic texture displayed by **1** in the mesophase at 150 °C.

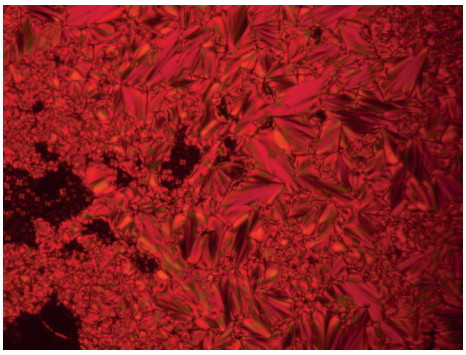

Figure 8. Thermal polarized optical micrograph of the focal-conic texture displayed by **5** in the mesophase at 170 °C.

sublayer between mesogenic and mixed liquid-like sublayers (Figure 10). Notably, the tilted phase could not be differentiated by SAXS and the narrow temperature-range of the N phase did not permit investigations.

Table 1. Phase-transition temperatures and enthalpies of the studied compounds.[a]

	T_g [°C]	Transition	T [°C]	ΔH [kJ mol^{-1}]
9	18	SmC→SmA	90[b]	–
		SmA→N	153	
		N→I	163	5.4[c]
11	47	SmA→I	149	11.6
15	24	SmA→N	168	
		N→I	172	8.8[c]
17	45	SmA→I	158	11.1
4	28	SmC→SmA	86[b]	–
		SmA→N	171	
		N→I	175	11.4[c]
2	42	SmC→SmA	90[b]	–
		SmA→I	156	18.3
3	42	SmC→SmA	90[b]	–
		SmA→I	156	17.8
1	44	SmA→I	168	25.3
6	38	SmA→N	171	
		N→I	180	16.3[c]
5	39	SmA→I	175	27.4

[a] T_g: glass transition temperature, SmA: smectic A phase, SmC: smectic C phase, N: nematic phase, I: isotropic liquid. [b] Observed by POM. [c] Overall enthalpy (broad transitions).

Table 2. Main characteristics of the mesophases displayed by cross-metathesis compounds and olefinic type I precursors.[a]

	T [°C]	Phase	V_{mol} [Å^3] (ρ [g cm^{-3}])	d [Å]	A_{mol} [Å^2]	a_{mes} [Å^2]	τ
1	100	SmA	6143 (1.21)	91.5 ± 1.5	67	33.5	0.56
	20	SmA	5795 (1.28)	89.4 ± 1.5	65	32.5	0.53
2	100	SmA	5395 (1.16)	97.6 ± 1.0	55	27.5	0.81
	20	SmA	5090 (1.23)	85.4 ± 0.8	60	30	0.65
3	100	SmA	5395 (1.16)	95.9 ± 1.0	56	28	0.79
	20	SmA	5090 (1.23)	82.7 ± 0.8	61	30.5	0.60
4	100	SmA	4648 (1.09)	93.8 ± 1.0	50	25	0.94
	20	Cr	–	–	–	–	–
5	100	SmA	9863 (1.17)	86.0 ± 0.6	115	28.75	0.77
	20	SmA	9305 (1.24)	83.7 ± 0.8	111	27.75	0.74
6	100	SmA	8369 (1.09)	52.3 ± 1.0	160	40	0.28
	20	amorphous	–	–	–	–	–
9	130	SmA	2424 (1.04)	80.7 ± 2.0	30	30	0.74
	100	SmA	2374 (1.06)	84.3 ± 2.0	28	28	0.79
	20	Cr	–	–	–	–	–
11	100	SmA	3122 (1.19)	93.1 ± 1.0	34	34	0.56
	20	SmA	2945 (1.26)	85.4 ± 0.8	35	35	0.43
15	100	SmA	4235 (1.08)	53.2 ± 0.4	80	40	0.29
	20	amorphous	–	–	–	–	–
17	100	SmA	4982 (1.16)	83.4 ± 0.6	60	30	0.72
	20	SmA	4700 (1.23)	82.4 ± 0.6	57	28.5	0.71

[a] SmA: smectic A phase, Cr: crystalline phase. V_{mol}: calculated molecular volume; ρ: density; d: lamellar periodicity; A_{mol}: molecular area ($A_{mol} = V_{mol}/d$); τ: bilayer ratio calculated from the mesogenic area, $a_{mes} = 2n_{mL}A_{mol}/n_{mes}$ (in which n_{mL} is the number of molecular layers per lamellar period; thus, $n_{mL} = 1$ for the cross-metathesis compounds and $n_{mL} = 2$ for the olefinic precursors, and n_{mes} is the number of mesogens per molecule for the cross-metathesis compounds or the total number of mesogens per dimer for the olefinic precursors),[38] and from the natural cross-sectional area of mesogens, $\sigma_{mes} \approx 23.3$ Å^2 at 100 °C (22 Å^2 at 20 °C), according to the equation $\tau = 2 - (a_{mes}/\sigma_{mes})$ (assuming untilted end mesogens in the sublayers). The volume of C_{60} was deduced from its crystalline structure (face-centered cubic (fcc) crystalline system with $a = 14.15$ Å, $\rho = 1.70$ g cm^{-3}, $Z = 4$);[39] volume of $C_{60} = 705$ Å^3.

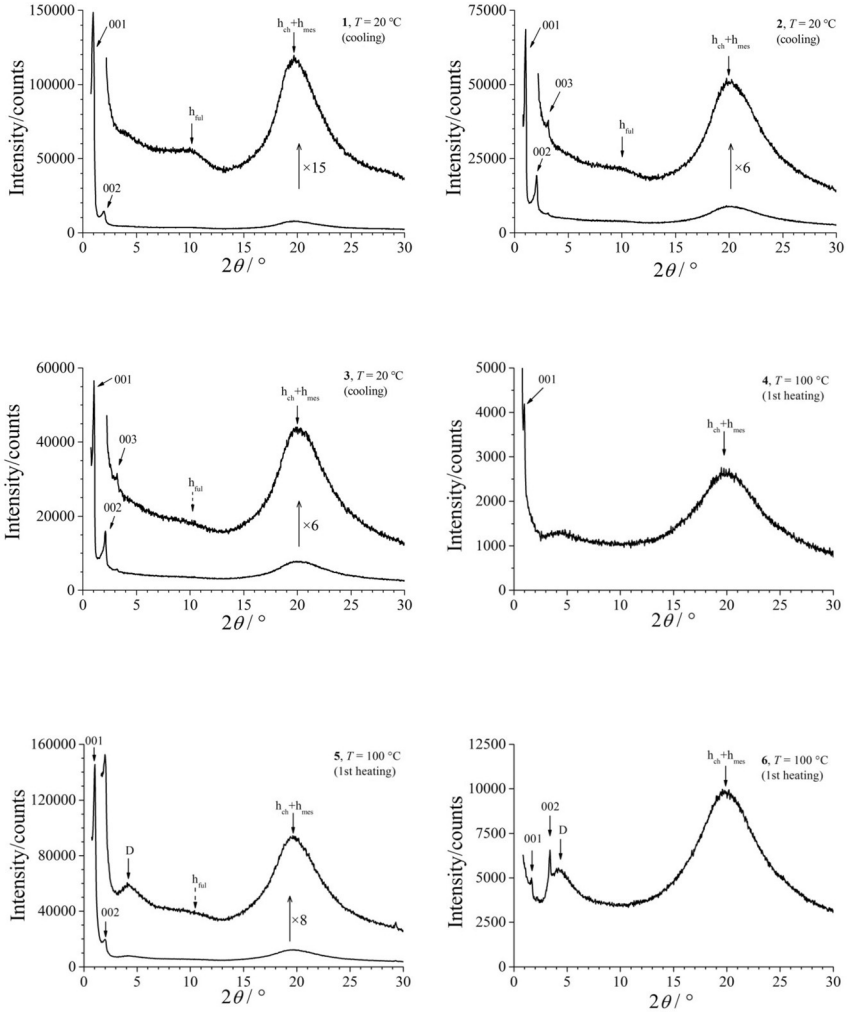

Figure 9. Representative SAXS patterns of the lamellar phases displayed by cross-metathesis compounds **1**–**6** (additional SAXS patterns are given in the Supporting Information).

Supramolecular organization

Two types of self-association mechanisms are usually considered in the case of systems containing polar mesogens, such as the CB ones: the mesogens can either self-organize head-to-head, leading to bilayered structures, or head-to-tail, giving rise to monolayers. The corresponding smectic organizations are actually intermediate between these two limit cases, with molecular areas per end-on mesogen, a_{mes}, ranging between one (bilayer) and two (monolayer) times the natural cross-section of the mesogen, σ_{mes}. A bilayer ratio parameter τ, which varies between zero (for monolayers) and one (for bilayers), can then be defined from the a_{mes}/σ_{mes} areas ratio (Table 2).[40] Both types of self-association compete in CB-based mesogens and lead to a wide-range variation of τ in the smectic phases, following small drifts in interactions between mesogens and chains. In multisegregated lamellar phases, the variation of τ provides an easy mechanism to adapt the natural cross-section of end groups to the compromise molecular area, A_{mol}, of the whole sequence of sublayers.[38] Accordingly, for first-generation malonates (**4** and **9**), which contain two CB end groups per linear segment of similar cross-section, a high degree of bilayering is promoted ($\tau = 0.7$–1.0). Expectedly, both linear segment lengths and mono- or bis-dendritic architectures lead to similar τ values, since these features barely influence the cross-section ratios. Regarding the dendritic units, the cross-sections of the first-generation compounds come down to a single phenyl ring with areas comparable to those of the linear segments, which therefore do not modify the balance with the terminal branches, and thus, limit the lateral expansion of the mesogenic bilayers. On the contrary, the dendritic units of higher generation acquire a wedge shape that facilitates a higher lateral expansion of the layers. This may be the reason for the observed drop of τ to 0.25–0.3 for the second-generation compounds (**15** and **6**), the relative lower influence of the linear segment, which also acts to reduce the proportion of bilayers. Finally, the connection of the CB mesogens to the higher generation dendritic units perturbs the formation of regular sublayers with sharp interfaces, as shown by the smaller number and lower intensity of the lamellar reflections. These perturbations persist with the rigidification of the sample upon cooling, leaving an amorphous room-temperature state with local-range nanosegregation. Patterns then

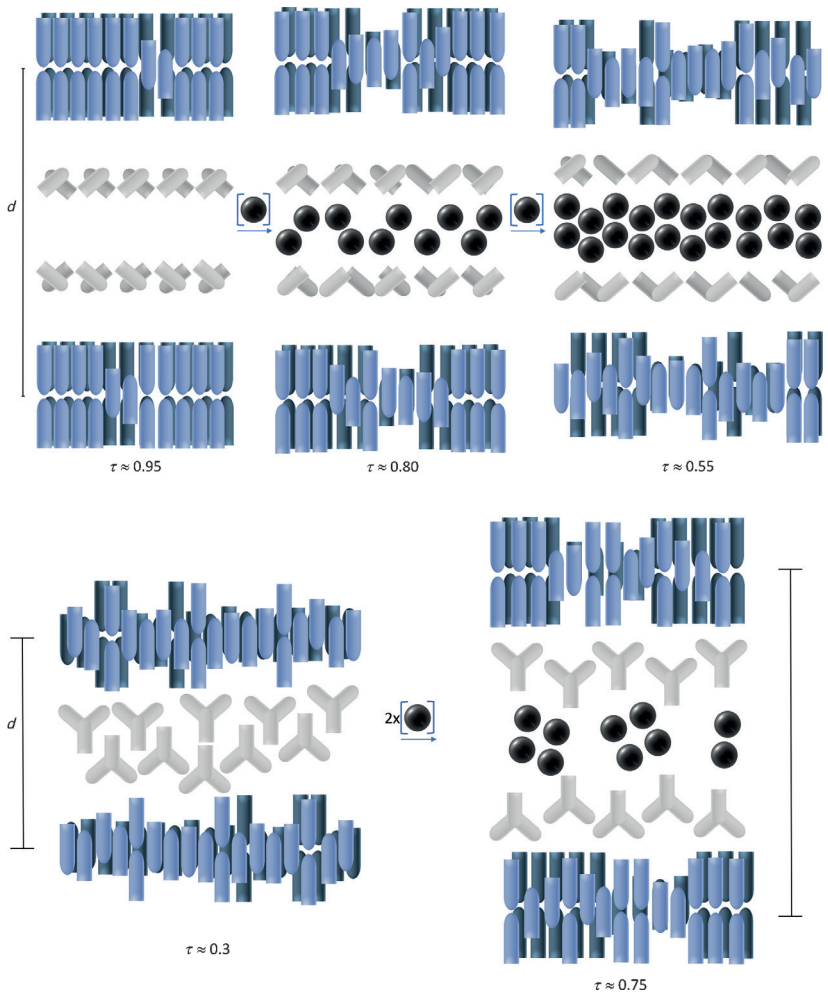

Figure 10. Schematic representation of the supramolecular lamellar organizations of compounds **1**–**4** (top) and **5**–**6** (bottom). Black balls: [60]fullerenes; blue cylinders: CB mesogens; gray cylinders: first-generation rigid connectors; gray Y shapes: second-generation rigid connectors; darker cylinders: mesogens from the back row; spacing between fullerene rows ($h_{ful} \approx 10$ Å) is about twice that of mesogen rows ($h_{mes} \approx 4.6$ Å). The molten aliphatic spacers, which fill the white spaces, are omitted for clarity.

only preserve the scattering signals around 4.5 and 20 Å from distances between alkyl chains, mesogens, and dendritic units.

The addition of C_{60} onto the malonate sites modifies the molecular packing in a different way for each generation of dendrimers. For the first-generation systems, the size of the C_{60} units ($\sigma_{ful} \approx 86$ Å^2) expands far beyond the overall cross-section of the end groups ($2\sigma_{mes} \approx 46$ Å^2) and the insertion of the [60]fullerene-containing strata inevitably causes a lateral expansion of the lamellae (Table 2 and Figure 10). The effect depends on the C_{60} content. The addition of only one of the two possible sites in this series of dendrimers increases the molecular area, A_{mol}, by only about 10% (from 50 Å^2 for **4** to ca. 55–56 Å^2 for **2** and **3**). This modest swelling implies that the additional substituent volume distributes between linear segments over a large portion of the sublayer, which is moreover confirmed by the absence of a long-range correlation signal between the C_{60} groups in the SAXS patterns (Figure 9). Despite its apparent looseness, the C_{60} strata retain the various constitutive molecular parts of the bis-malonate **4** in specific sublayers and add intermediate high-electron-density layers, which explains the increased number of lamellar reflections and weakened first-order reflections. The subsequent addition of C_{60} onto the second malonate site causes more substantial lateral expansions ($nA_{mol} = 65$–70 Å^2 for **1** ($n = 1$) and tail-to-tail "dimer" **11** ($n = 2$)), which stay, however, far below the total area requirement of the linear segment and [60]fullerene ($\sigma_{ful} + \sigma_{lin} \approx 108$ Å^2). Neighboring [60]fullerenes are therefore still loosely intercalated, although the appearance of a broad scattering maximum, $h_{ful} \approx 10$ Å, reveals the onset of positional correlations between them.

For the second-generation dendrimers, the molecular area of bis-malonate **6** ($A_{mol} \approx 160$ Å^2) far exceeds the overall cross-section of the substituted linear segment (see above). Contrary to the lower-generation adducts, for which insertion of C_{60} causes lateral expansion, the formation of a compact strata of aggregated [60]fullerenes in the second-generation materials therefore requires a reduction of the molecular area with respect to bis-malonate **6**. Shrinkage toward molecular areas close to $\sigma_{ful} + \sigma_{lin}$ is indeed observed for the three adducts (A_{mol}(dimer: $2A_{mol}$) = 110–120 Å^2 for **5** and **17**), which means

that the constraints at the origin of the expansion in **5** and **17** have been overcome. In other words, the compactness of packing now appears to be ruled by the space requirements of the C_{60} strata, whereas the dendritic moieties adapt and the CB groups simply disentangle, passing from being mainly monolayer-like ($\tau \approx 0.3$) to mainly bilayer-like ($\tau \approx 0.7$–0.75). Presumably, lateral shrinking (and related longitudinal expansion) of the dendritic moieties is facilitated by their wedge shape, which results in more compact packing through a simple longitudinal shift between neighboring molecules; the free space between wedges is filled with molten aliphatic spacers. Geometrically, this shift is comparable to partial bilayering and can be appreciated by using the same approach as that for the CB arrangement through the introduction of a further bilayering ratio parameter, that is, $\tau_{den} = 2[1-(A_{mol}/\sigma_{den})]$, in which $\sigma_{den} \approx 160$ Å^2 represents the full extension of the wedges in compound **6**. Consistently, this description results in τ_{den} ratios lying between 0.5 and 0.6 for compounds **5** and **17** (τ_{den} for second-generation fullerene derivatives = 0), which highlights the deleterious effect on the formation of regular sublayers with sharp interfaces and explains the weakness of lamellar reflections in the mesophase and amorphous room-temperature state. Finally, as observed by POM, only the [60]fullerene-free compounds exhibit a nematic phase, which forms at a higher temperature than the clearing transition temperatures of the [60]fullerene adducts. This result agrees well with the strong interactions that prevail in the sublayers between the C_{60} moieties, which permit the strong cohesion of the lamellar phase of the adducts, but which also coexist with strong perturbations of the layers caused by the bulky C_{60} units. When these interactions weaken as the temperature increases, the systems directly melt into the isotropic phase because lateral associations are sterically hindered, whereas, in the case of the [60]fullerene-free materials, some interactions may be preserved to give rise to a nematic organization.

In summary, the lamellar packing seems to be mainly controlled by the dendritic moiety in the bis-malonates **4** and **6**. In the multisegregated lamellae, the self-organization of the [60]fullerene becomes predominant. The stability of the mesophases and structural parameters depend on a subtle interplay of attractive interactions between neighboring fullerenes and steric hindrance (bulkiness of C_{60} and dendritic parts) that can be modulated by molecular design of the bis-malonate addends (e.g., generation of the dendron, spacer, malonate sites). In the case of multiblock compounds, such as the above-described bis-[60]fullerodendrimers or other complicated structures,[33,36,37] the mesophases may not be strictly referred to as the smectic phases found in classical thermotropic mesogens because of the median intermediary strata of C_{60}. To highlight this difference (i.e., the multilayered character combined with the mesogenic layers), we propose to label such mesophases multilayered SmA/C phases.

Conclusions

The olefin cross-metathesis reaction was successfully applied for the efficient construction of bis-[60]fullerodendrimers. First- and second-generation poly(aryl ester) dendrons carrying CB mesogens were used as liquid-crystalline promoters. Connection of type I (terminal olefin) and type II (α,β-unsaturated carbonyl olefin) olefinic precursors under standard conditions and in the presence of second-generation Grubbs catalysts gave the desired cross-metathesis compounds, for which the *E* configuration in the newly formed carbon–carbon double bond was established by ^{1}H NMR spectroscopy. The modular synthetic approach developed herein also allowed the synthesis of mono-[60]fullerodendrimers and their [60]fullerene-free analogues.

All compounds gave rise to the formation of SmA/C ([60]fullerene-free materials) or multilayered SmA (C_{60} derivatives) phases. The emergence of these mesophases is in agreement with the presence of terminal CB mesogens that tend to arrange into layers, whereas the multiblock architecture of the [60]fullerodendrimers further implies the segregation of various molecular constituents into multisegregated lamellar phases. The supramolecular organization is controlled by the subtle interplay of the main constitutive molecular parts; the CB mesogens adapt their space requirements towards the bulky ones (e.g., dendritic moieties, C_{60}) by varying the proportion of mono- and bilayer arrangements in the multisegregated lamellae.

Finally, the synthetic approach reported herein represents a general concept that can be easily applied to the design of complex supramolecular materials based on many different functional units.

Acknowledgements

R.D. thanks the Swiss National Science Foundation (grant no. 200020-140298 and 200020-152716) for financial support. B.D. and B.H. thank the CNRS for financial support.

Keywords: dendrimers · fullerenes · liquid crystals · metathesis · self-assembly

[1] a) E. Busseron, Y. Ruff, E. Moulin, N. Giuseppone, *Nanoscale* **2013**, *5*, 7098 – 7140; b) M. J. Hollamby, M. Karny, P. H. H. Bomans, N. A. J. M. Sommerdjik, A. Saeki, S. Seki, H. Minamikawa, I. Grillo, B. R. Pauw, P. Brown, J. Eastoe, H. Möhwald, T. Nakanishi, *Nat. Chem.* **2014**, *6*, 690 – 696; c) J.-M. Lehn, *Angew. Chem. Int. Ed.* **2015**, *54*, 3276 – 3289; *Angew. Chem.* **2015**, *127*, 3326 – 3340.

[2] D. M. Guldi, B. M. Illescas, C. M. Atienza, M. Wielopolski, N. Martín, *Chem. Soc. Rev.* **2009**, *38*, 1587 – 1597.

[3] L. Echegoyen, L. E. Echegoyen, *Acc. Chem. Res.* **1998**, *31*, 593 – 601.

[4] P. Anilkumar, F. Lu, L. Cao, P. G. Luo, J.-H. Liu, S. Sahu, K. N. Tackett II, Y. Wang, Y.-P. Sun, *Curr. Med. Chem.* **2011**, *18*, 2045 – 2059.

[5] Y. Chen, D. Zhao, Y. Liu, *Chem. Commun.* **2015**, *51*, 12266 – 12269.

[6] a) P. Compain, C. Decroocq, J. Iehl, M. Holler, D. Hazelard, T. Mena Barragán, C. Ortiz Mellet, J.-F. Nierengarten, *Angew. Chem. Int. Ed.* **2010**, *49*, 5753 – 5756; *Angew. Chem.* **2010**, *122*, 5889 – 5892; b) T. A. Strom, S. Durdagi, S. S. Ersoz, R. E. Salmas, C. T. Supuran, A. R. Barron, *J. Pept. Sci.* **2015**, *21*, 862 – 870.

[7] A. Muñoz, D. Sigwalt, B. M. Illescas, J. Luczkowiak, L. Rodríguez-Pérez, I. Nierengarten, M. Holler, J.-S. Remy, K. Buffet, S. P. Vincent, J. Rojo, R. Delgado, J.-F. Nierengarten, N. Martín, *Nat. Chem.* **2015**, *7*, 50 – 57.

[8] V. Vorobyov, V. Kaptsov, R. Gordon, E. Makarova, I. Podolski, F. Sengpiel, *J. Alzheimer's Dis.* **2015**, *45*, 217 – 233.

[9] V. V. Kleandrova, F. Luan, A. Speck-Planche, M. N. D. S. Cordeiro, *Curr Bioinform.* **2015**, *10*, 565 – 578.

[10] a) T. Torres, A. Gouloumis, D. Sanchez-Garcia, J. Jayawickramarajah, W. Seitz, D. M. Guldi, J. L. Sessler, *Chem. Commun.* **2007**, 292 – 294; b) T. M. Figueira-Duarte, A. Gégout, J.-F. Nierengarten, *Chem. Commun.* **2007**, 109 – 119; c) Y. Hizume, K. Tashiro, R. Charvet, Y. Yamamoto, A. Saeki, S. Seki, T. Aida, *J. Am. Chem. Soc.* **2010**, *132*, 6628 – 6629; d) B. Pelado, F. Abou-Chahine, J. Calbo, R. Caballero, P. de La Cruz, J. M. Junquera-Hernández, E. Ortí, N. V. Tkachenko, F. Langa, *Chem. Eur. J.* **2015**, *21*, 5814 – 5825.

[11] G. de La Torre, F. Giacalone, J. L. Segura, N. Martín, D. M. Guldi, *Chem. Eur. J.* **2005**, *11*, 1267 – 1280.

[12] S. Fukuzumi, K. Ohkubo, *Dalton Trans.* **2013**, *42*, 15846 – 15858.

[13] a) Y. Li, *Acc. Chem. Res.* **2012**, *45*, 723 – 733; b) Y. Liu, J. Zhao, Z. Li, C. Mu, W. Ma, H. Hu, K. Jiang, H. Lin, H. Ade, H. Yan, *Nat. Commun.* **2014**, *5*, 5293; c) Y. Lin, J. Wang, Z.-G. Zhang, H. Bai, Y. Li, D. Zhu, X. Zhan, *Adv. Mater.* **2015**, *27*, 1170 – 1174.

[14] a) K. Lee, Y. J. Choi, Y.-J. Cho, C. Y. Lee, H. Song, C. H. Lee, Y. S. Lee, J. T. Park, *J. Am. Chem. Soc.* **2004**, *126*, 9837 – 9844; b) S. R. Plant, M. Jevric, J. J. L. Morton, A. Ardavan, A. N. Khlobystov, G. A. D. Briggs, K. Porfyrakis, *Chem. Sci.* **2013**, *4*, 2971 – 2975; c) Y. Abe, H. Tanaka, Y. Guo, Y. Matsuo, E. Nakamura, *J. Am. Chem. Soc.* **2014**, *136*, 3366 – 3369; d) P. Moreno-García, A. La Rosa, V. Kolivoška, D. Bermejo, W. Hong, K. Yoshida, M. Baghernejad, S. Filippone, P. Broekmann, T. Wandlowski, N. Martín, *J. Am. Chem. Soc.* **2015**, *137*, 2318 – 2327.

[15] a) M. Prato, *J. Mater. Chem.* **1997**, *7*, 1097 – 1109; b) G. P. Miller, J. Briggs, *Org. Lett.* **2003**, *5*, 4203 – 4206.

[16] a) C. M. Atienza, G. Fernández, L. Sánchez, N. Martín, I. Sá Dantas, M. M. Wienk, R. A. J. Janssen, G. M. Aminur Rahman, D. M. Guldi, *Chem. Commun.* **2006**, 514 – 516; b) G. Fernández, L. Sánchez, D. Veldman, M. M. Wienk, C. Atienza, D. M. Guldi, R. A. J. Janssen, N. Martín, *J. Org. Chem.* **2008**, *73*, 3189 – 3196.

[17] a) K. Hosomizu, H. Imahori, U. Hahn, J.-F. Nierengarten, A. Listorti, N. Armaroli, T. Nemoto, S. Isoda, *J. Phys. Chem. C* **2007**, *111*, 2777 – 2786; b) U. Hahn, J.-F. Nierengarten, F. Vögtle, A. Listorti, F. Monti, N. Armaroli, *New J. Chem.* **2009**, *33*, 337 – 344; c) J. Kim, M. H. Yun, J. Lee, J. Y. Kim, F. Wudl, C. Yang, *Chem. Commun.* **2011**, *47*, 3078 – 3080; d) F. Hörmann, A. Hirsch, *Chem. Eur. J.* **2013**, *19*, 3188 – 3197.

[18] N. Zhou, L. Wang, D. W. Thompson, Y. Zhao, *Tetrahedron Lett.* **2007**, *48*, 3563 – 3567.

[19] J. K. Sørensen, J. Fock, A. H. Pedersen, A. B. Petersen, K. Jennum, K. Bechgaard, K. Kilså, V. Geskin, J. Cornil, T. Bjørnholm, M. Brøndsted Nielsen, *J. Org. Chem.* **2011**, *76*, 245 – 263.

[20] a) C. Bingel, *Chem. Ber.* **1993**, *126*, 1957 – 1959; b) J.-P. Bourgeois, F. Diederich, L. Echegoyen, J.-F. Nierengarten, *Helv. Chim. Acta* **1998**, *81*, 1835 – 1844; c) J.-F. Nierengarten, V. Gramlich, F. Cardullo, F. Diederich, *Angew. Chem. Int. Ed. Engl.* **1996**, *35*, 2101 – 2103; *Angew. Chem.* **1996**, *108*, 2242 – 2244.

[21] a) P. N. Confalone, E. M. Huie, *J. Org. Chem.* **1983**, *48*, 2994 – 2997; b) M. Prato, M. Maggini, *Acc. Chem. Res.* **1998**, *31*, 519 – 526; c) N. Tagmatarchis, M. Prato, *Synlett* **2003**, 768 – 779.

[22] a) T. Nakanishi, *Chem. Commun.* **2010**, *46*, 3425 – 3436; b) S. S. Babu, H. Möhwald, T. Nakanishi, *Chem. Soc. Rev.* **2010**, *39*, 4021 – 4035.

[23] a) P. A. L. Fernandes, S. Yagai, H. Möhwald, T. Nakanishi, *Langmuir* **2010**, *26*, 4339 – 4345; b) H. Li, S. S. Babu, S. T. Turner, D. Neher, M. J. Hollamby, T. Seki, S. Yagai, Y. Deguchi, H. Möhwald, T. Nakanishi, *J. Mater. Chem. C* **2013**, *1*, 1943 – 1951.

[24] a) S. Campidelli, T. Brandmüller, A. Hirsch, I. M. Saez, J. W. Goodby, R. Deschenaux, *Chem. Commun.* **2006**, 4282 – 4284; b) H. Mamlouk, B. Heinrich, C. Bourgogne, B. Donnio, D. Guillon, D. Felder-Flesch, *J. Mater. Chem.* **2007**, *17*, 2199 – 2205; c) S. Guerra, J. Iehl, M. Holler, M. Peterca, D. A. Wilson, B. E. Partridge, S. Zhang, R. Deschenaux, J.-F. Nierengarten, V. Percec, *Chem. Sci.* **2015**, *6*, 3393 – 3401.

[25] K. Toth, J. K. Molloy, M. Matta, B. Heinrich, D. Guillon, G. Bergamini, F. Zerbetto, B. Donnio, P. Ceroni, D. Felder-Flesch, *Angew. Chem. Int. Ed.* **2013**, *52*, 12303 – 12307; *Angew. Chem.* **2013**, *125*, 12529 – 12533.

[26] W.-S. Li, Y. Yamamoto, T. Fukushima, A. Saeki, S. Seki, S. Tagawa, H. Masunaga, S. Sasaki, M. Takata, T. Aida, *J. Am. Chem. Soc.* **2008**, *130*, 8886 – 8887.

[27] J. Vergara, J. Barberá, J. L. Serrano, M. B. Ros, N. Sebastián, R. de La Fuente, D. O. López, G. Fernández, L. Sánchez, N. Martín, *Angew. Chem. Int. Ed.* **2011**, *50*, 12523 – 12528; *Angew. Chem.* **2011**, *123*, 12731 – 12736.

[28] M. Lehmann, M. Hügel, *Angew. Chem. Int. Ed.* **2015**, *54*, 4110 – 4114; *Angew. Chem.* **2015**, *127*, 4183 – 4187.

[29] C.-L. Wang, W.-B. Zhang, C.-H. Hsu, H.-J. Sun, R. M. Van Horn, Y. Tu, D. V. Anokhin, D. A. Ivanov, S. Z. D. Cheng, *Soft Matter* **2011**, *7*, 6135 – 6143.

[30] A. K. Chatterjee, T.-L. Choi, D. P. Sanders, R. H. Grubbs, *J. Am. Chem. Soc.* **2003**, *125*, 11360 – 11370.

[31] T. M. N. Trinh, T. T. Nguyen, C. Kopp, P. Pieper, V. Russo, B. Heinrich, B. Donnio, T. L. A. Nguyen, R. Deschenaux, *Eur. J. Org. Chem.* **2015**, 6005 – 6010.

[32] T. T. Nguyen, T. L. A. Nguyen, R. Deschenaux, *J. Porphyrins Phthalocyanines* **2016**; DOI: 10.1142/S1088424616500504.

[33] S. Campidelli, J. Lenoble, J. Barberá, F. Paolucci, M. Marcaccio, D. Paolucci, R. Deschenaux, *Macromolecules* **2005**, *38*, 7915 – 7925.

[34] K. Voigtritter, S. Ghorai, B. H. Lipshutz, *J. Org. Chem.* **2011**, *76*, 4697 – 4702.

[35] a) B. Ma, C. E. Bunker, R. Guduru, X.-F. Zhang, Y.-P. Sun, *J. Phys. Chem. A* **1997**, *101*, 5626 – 5632; b) F. Cardullo, P. Seiler, L. Isaacs, J.-F. Nierengarten, R. F. Haldimann, F. Diederich, T. Mordasini-Denti, W. Thiel, C. Boudon, J.-P. Gisselbrecht, M. Gross, *Helv. Chim. Acta* **1997**, *80*, 343 – 371; c) D. M. Guldi, *Chem. Commun.* **2000**, 321 – 327.

[36] A. Pitto-Barry, P. E. N. Barry, V. Russo, B. Heinrich, B. Donnio, B. Therrien, R. Deschenaux, *J. Am. Chem. Soc.* **2014**, *136*, 17616 – 17625.

[37] R. Deschenaux, B. Donnio, D. Guillon, *New J. Chem.* **2007**, *31*, 1064 – 1073.

[38] Z. T. Nagy, B. Heinrich, D. Guillon, J. Tomczyk, J. Stumpe, B. Donnio, *J. Mater. Chem.* **2012**, *22*, 18614 – 18622.

[39] T. Kitamoto, S. Sasaki, T. Atake, T. Tanaka, H. Kawaji, K. Kikuchi, K. Saito, S. Suzuki, Y. Achiba, I. Ikemoto, *Jpn. J. Appl. Phys.* **1993**, *32*, L424 – 427.

[40] a) D. Guillon, A. Skoulios, *Mol. Cryst. Liq. Cryst.* **1983**, *91*, 341 – 352; b) D. Guillon, A. Skoulios, *J. Phys.* **1984**, *45*, 607 – 624; c) T. Cardinaels, K. Driesen, T. N. Parac-Vogt, B. Heinrich, C. Bourgogne, D. Guillon, B. Donnio, K. Binnemans, *Chem. Mater.* **2005**, *17*, 6589 – 6598.